Zhou
Protection and Control of Modern Power Systems (2022) 7:37
https://doi.org/10.1186/s41601-022-00257-8

Protection and Control of Modern Power Systems

ORIGINAL RESEARCH Open Access

Drive-train torsional vibration suppression of large scale PMSG-based WECS

Feihang Zhou*

Abstract

This paper provides a systematic analysis of the large scale PMSG (permanent magnet synchronous generator)-based WECS (wind energy conversion system) torsional vibration problem under MPPT (maximum power point tracking) control and constant power control. This is from the perspective of SSO (sub-synchronous oscillation), SSH (sub-synchronous harmonics) and forced torsional vibration. The cause of SSO is the negative total system damping, weakened by the constant power control. The system is susceptible to inducing SSH in the grid current and voltage in the under-damped condition. To effectively suppress the torsional vibration of PMSG-based WECS, a stiffness compensation control strategy based on adaptive damping is proposed. The results show that SSO, SSH and the forced torsional vibration can be suppressed at the source using the proposed suppression strategy.

Keywords: Adaptive damping, Constant power control, MPPT, PMSG-based WECS, SSH, SSO, Stiffness compensation, Torsional vibration

1 Introduction

Torsional vibration can cause severe damage to a drive-train and can also lead to problems of SSO (sub-synchronous oscillation) and SSH (sub-synchronous harmonics) in a power system. In December 1970 and October 1971, two serious torsional vibration accidents occurred in the steam turbine units' shaft in the Mohave power plant in the United States, causing damage to the generator shaft [1]. The cause of the two accidents was SSR (sub-synchronous resonance) produced by the interaction between the torsional vibration of the steam turbine shaft and the series compensation capacitance of the transmission system. Subsequently, in 1977, it was found that an HVDC transmission system could also cause strong steam turbine torsional vibration [2, 3]. Compared with the torsional vibration caused by series compensation capacitance, the torsional vibration caused by HVDC cannot form a resonant loop. Therefore, the mechanisms of these two torsional vibrations are different, though they have been collectively referred to as SSO. Compared with SSR, SSO has a broader meaning and there have been many forms of SSO, although SSO involved in torsional vibration is still the major form. It can be seen that torsional vibration is a historical issue, and the early concern of SSO was caused by steam turbine unit torsional vibration.

In recent years, the development of renewable energy, e.g., wind energy, has made great progress [4, 5] and wind turbines are becoming larger. However, with larger wind turbine size and capacity, the torsional vibration problem is becoming increasingly prominent.

1.1 Harm of torsional vibration

Torsional vibration can seriously harm equipment and the connected power system as follows:

1) Torsional vibration can aggravate the fatigue damage of a shaft. From the mechanics of materials, when torsional vibration occurs on a shaft, it is equivalent to imposing an alternating periodic stress on the shaft. Both the amplitude and frequency of the stress can affect the fatigue life of the shaft. The torsional

*Correspondence: qq987102679@126.com; zhoufeihang@xupt.edu.cn

School of Automation, Xi'an University of Posts & Telecommunications, Chang'an West St. Chang'an District, Xi'an 710121, China

Springer Open

© The Author(s) 2022. **Open Access** This article is licensed under a Creative Commons Attribution 4.0 International License, which permits use, sharing, adaptation, distribution and reproduction in any medium or format, as long as you give appropriate credit to the original author(s) and the source, provide a link to the Creative Commons licence, and indicate if changes were made. The images or other third party material in this article are included in the article's Creative Commons licence, unless indicated otherwise in a credit line to the material. If material is not included in the article's Creative Commons licence and your intended use is not permitted by statutory regulation or exceeds the permitted use, you will need to obtain permission directly from the copyright holder. To view a copy of this licence, visit http://creativecommons.org/licenses/by/4.0/.

vibration of high-speed PMSG-based WECS (Wind Energy Conversion System) is very serious, because its drive-train contains some flexible components such as gearbox and flexible coupling. In many field accidents, gearbox damage and coupling skidding account for a large proportion of the damage.

2) Torsional vibration can cause SSO and potentially make the system lose stability. As in a steam turbine unit, a DFIG (doubly fed induction generator)-based WECS also adopts a direct grid connection mode. Therefore, the SSO mechanisms of DFIG-based WECS and a steam turbine unit are similar. There is currently a lot of research on the SSO problem of DFIG-based WECS [6–9]. Because a PMSG-based WECS uses an inverter grid-connected mode it removes the direct connection between generators and power grid. Therefore, the SSO problem of PMSG-based WECS may depend only on the generator control mode. There has also been research showing that power control can weaken system damping and even induce SSO in a PMSG-based WECS.
3) Torsional vibration is the main source of SSH. In fact, for power systems containing wind power generation, it is worth noting that all disturbances, including wind, can cause a WECS to produce torsional vibrations in the sub-synchronous frequency range. Low-intensity torsional vibration may only have a small impact on the unit itself, but it may still cause sub-synchronous frequency oscillation of electrical parameters such as grid current or voltage. IEEE generally uses "sub-synchronous frequency components" or "SSH" to describe this electrical oscillation. As the wind power penetration increases, a large amount of SSH is transmitted between the power grid sources. This may cause other forms of SSO. On July 1, 2015, a wind farm in Hami, Xinjiang, China produced a large amount of SSH. After 5 levels of transformation, the SSH was transmitted to the thermal power unit 300 km away and triggered the torsional vibration protection action of three sets of the 660 MW units of the garden power plant. The units were successively tripped and the power plant was completely shut down. On examination, there was a large direct-driven wind farm connected to the adjacent power grid. Many SSH close to the natural frequencies of the thermal power units shafts were generated by the PMSG-based WECS, and these were transferred to the thermal power plant through the grid and subsequently caused the severe torsional vibration of the thermal power units. There have been some similar accidents in Texas, USA and Guyuan County in Hebei Province, China. The above accidents indicate that the monitoring of SSH in the power grid has been insufficient and generally SSH in wind farms has been neglected.

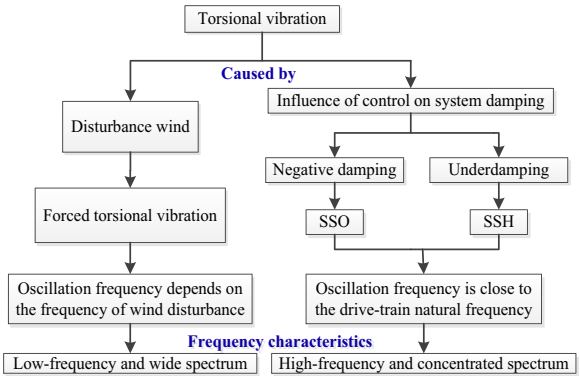

Fig. 1 Causes and characteristics of torsional vibration

1.2 Causes and characteristics of torsional vibration

The causes and characteristics of torsional vibration are shown in Fig. 1. As shown, torsional vibration is mainly caused by wind disturbance and the influence of control on system damping. As the external disturbance source, persistent wind disturbance can excite the system and cause forced torsional vibration. The frequency of this forced torsional vibration depends on the wind disturbance frequency, while tower shadow effect, wind shear and turbulence should also be taken into account. The spectrum of wind disturbance is wide, and the frequency of wind disturbance is lower than the drive-train natural frequency. In addition, the control function may change the system damping. If the total damping of the system becomes negative, the system will exhibit unstable torsional oscillation, indicating SSO in the system. Moreover, the system is susceptible to external disturbances in under-damped conditions. This can induce torsional vibration near the drive-train natural frequency, while the underdamped torsional vibration can cause SSH. It is clear that the frequencies of both SSO and SSH are close to the drive-train natural frequency and the spectrum of oscillations is concentrated.

1.3 Research status of torsional vibration suppression

For torsional vibration suppression, damping control is considered an effective strategy. Steam turbine units and DFIG-based WECS can usually add active damping control to excitation links to improve system damping. However, PMSG-based WECS cannot perform excitation control because of its permanent magnet rotor. For this reason, a torsional vibration suppression strategy was proposed in [10, 11]. This added active damping control

to the generator torque control loop, and this method has been widely used in practice. The method needs to extract the torsional vibration information from the generator speed by a BPF (band-pass filter), and then multiply it by a magnification factor (or damping coefficient) as the damping compensation torque into the torque control loop [10–17]. However, the effectiveness of the BPF is affected by parameter uncertainties. In order to restore the performance of the damper, it is usually necessary to repeatedly adjust the parameters during the testing phase of the wind turbine to achieve a good matching effect. To overcome this problem, a damper based on an adaptive Kalman filter was proposed in [18], while a method for reconstructing DC-Link current to extract torsional vibration signals was proposed in [19–21]. The method was further simplified in [22, 23], which also pointed out that the torsional vibration signal could be extracted from the fluctuation of the DC-Link current. The effectiveness of the scheme was verified by experiment. In addition, there have been many studies on the torsional vibration suppression scheme of a WECS drive-train. SMC (sliding mode control) was applied to the suppression of torsional vibration in [24] and a good suppression effect was obtained. Reference [25] proposed a virtual inertia control method to suppress drive-train torsional vibration, while [26] proposed a SDDC (speed difference damping controller) to reduce the torsional vibration of the driveline. However, the methods in [24–26] were also based on BPF for extracting the torsional vibration information.

1.4 Existing problems of torsional vibration

Although SSO may occur in a PMSG-based WECS under power control, its mechanism is not clear. It is not conclusively determined whether PMSG-based WECS has the possibility to generate SSO under other control modes such MPPT control. Furthermore, the mechanism of SSH generated by torsional vibration also has not been understood. Thus, further research and discussion are required on effective suppression methods for forced torsional vibration caused by wind disturbance.

1.5 Main contributions and highlighted innovations

This paper focuses on the torsional vibration of a PMSG-based WECS in the two main control modes, i.e., MPPT control mode and constant power control mode, and provides an in-depth analysis of SSO, SSH and forced torsional vibration problems. The main contributions and innovations are as follows:

1) The mechanism of SSO is thoroughly explored. The study finds that power control can weaken system damping, and when the total damping becomes negative, SSO will occur. However, an MPPT strategy with OTC (optimal torque control) can increase the system damping and thus, SSO under MPPT control does not occur. Therefore, damping control must be adopted in the constant power mode. In addition, for conventional damping control, if the added damping is insufficient, the system will be in the under-damped state and SSH can be generated.
2) The mechanism of SSH is also analyzed in detail. The study finds that conventional control can usually result in a under-damped system which is susceptible to external disturbances to produce SSH.
3) A new stiffness compensation control strategy based on adaptive damping is proposed to reduce forced torsional vibration. Detailed analysis, design and simulation experiments are provided to verify the correctness of the strategy.

2 Mathematical model of PMSG-based WECS

A typical configuration of a generic 2 MW PMSG-based WECS is shown in Fig. 2. It mainly consists of a wind turbine, a flexible drive-train and an electrical system including a PMSG, two back-to-back connected VSCs (voltage source converters) comprised of a MSC (machine side converter), a DC-Link and a GSC (grid side converter), and the control system. The system components are implemented in Simulink and the parameters are given in the Appendix.

2.1 Wind turbine model

According to the Betz theory, the mechanical power absorbed by a wind turbine [27–31] is given by:

$$P_{tur} = 0.5\pi\rho R^2 C_P v^3 \tag{1}$$

where the subscript *tur* refers to wind turbine. ρ is air density, R is radius of wind turbine, v is wind speed, β is pitch angle, λ is TSR (tip-speed ratio), C_p is defined as the wind energy conversion coefficient. Usually, C_p is a function of β and λ, and λ is given by:

$$\lambda = R \cdot \omega_{tur} / v \tag{2}$$

where ω_{tur} is rotor speed. From (1) and (2), the aerodynamic torque of wind turbine is:

$$T_{tur} = P_{tur} / \omega_{tur} = 0.5\pi\rho R^5 C_P \omega_{tur}^2 \Big/ \lambda^3 \tag{3}$$

2.2 Flexible drive-train model

Because of the heavy load on a large-scale wind turbine drive-train, its resonance mode must be considered. In general, there are two methods for flexible drive-train modeling:

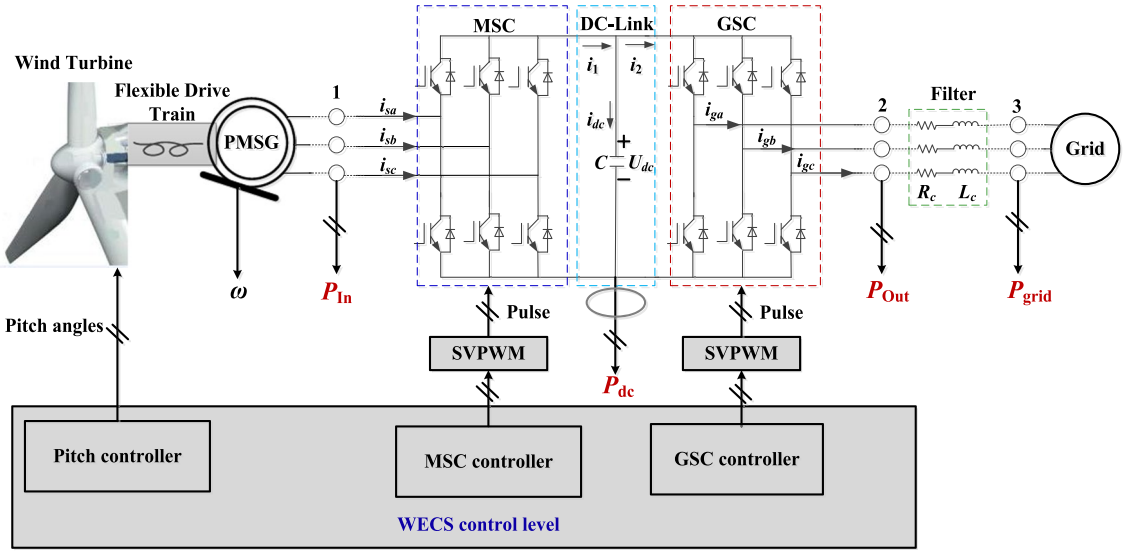

Fig. 2 A typical configuration of a generic 2 MW PMSG-based WECS

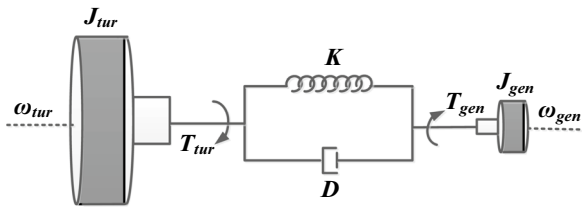

Fig. 3 Two-mass spring damping model

1) Continuous mass spring damping model. This model can accurately reflect the drive-train dynamics, but the solution process is very complicated.
2) Segmented concentrated mass spring damping model. This can be regarded as a simplified model. If the mass block is appropriately selected, the drive-train dynamics can also be well reflected. Therefore, this method is widely used.

For a PMSG-based WECS, both the wind turbine and generator can be considered as a single mass block. Thus, its flexible drive-train is usually described by the two-mass spring damping model shown in Fig. 3.

The flexible drive-train dynamic model [30] is expressed as:

$$J_{tur}\dot{\omega}_{tur} = -D(\omega_{tur} - \omega_{gen}) - K\theta + T_{tur} \tag{4a}$$

$$J_{gen}\dot{\omega}_{gen} = D(\omega_{tur} - \omega_{gen}) + K\theta - T_{gen} \tag{4b}$$

$$\dot{\theta} = \omega_{tur} - \omega_{gen} \tag{4c}$$

where the subscript *gen* refers to generator. J_{tur} is wind turbine rotational inertia, J_{gen} is generator rotational inertia, ω_{gen} is generator speed, T_{gen} is electromagnetic torque, θ is drive-train twist angle, K is drive-train stiffness coefficient, D is the drive-train damping.

2.3 Electrical system model

Figure 4 shows the control block of a full power converter. The purpose of MSC control is to realize the control of generator torque, while GSC control stabilizes the DC-Link voltage U_{dc} at its reference value U_{dc_ref} and achieves the necessary reactive power support for grid.

As described in [32], the PMSG model and MSC dynamics can be regarded as a first-order inertia link after inner-loop current feed-forward decoupling control and first-order tuning for the inner-loop current PI parameters, while the inertia delay of torque control can be adjusted by the PI parameters shown in Fig. 4(a). If the PI parameters are large enough, the dynamic delay of the torque loop can be neglected. Because MPPT control is generally used below rated wind speed v_{rate} and constant power control is adopted above v_{rate}, the electromagnetic torque T_{gen} is:

$$T_{gen} \approx T_{ref} = \begin{cases} K_{opt}\omega_{gen}^2 & v < v_{rate} \\ P_{rate}/\omega_{gen} & v \geq v_{rate} \end{cases} \quad \text{with } K_{opt} = \frac{\pi\rho R^5 C_{P\_max}}{2\lambda_{opt}^3} \tag{5}$$

where T_{ref} is the torque command, P_{rate} is the rated power, C_{P_max} is the maximum C_P and λ_{opt} is OTSR (optimal tip-speed ratio). In this paper, $C_{P\_max} = 0.48$ and $\lambda_{opt} = 8$.

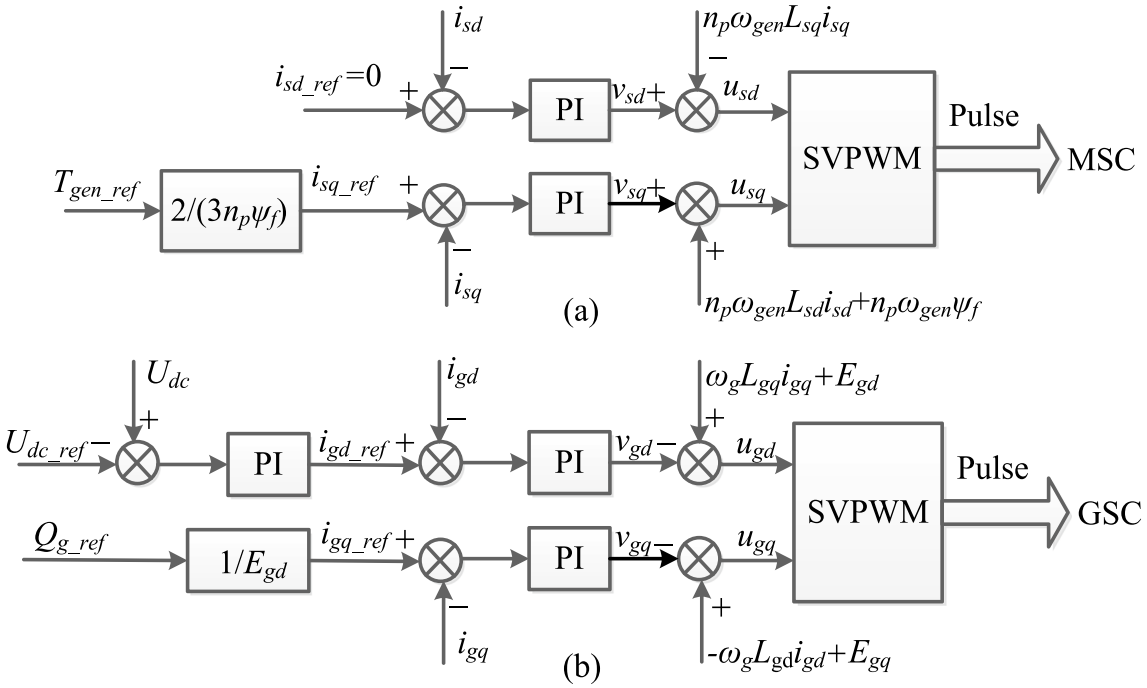

Fig. 4 Control block of a full power converter. **a** MSC control. **b** GSC control

3 Torsional vibration analyses

3.1 SSO problem discussion

As is well-known, PMSG-based WECS torsional vibration is mainly caused by wind disturbance and generator control, and is less affected by the power grid because of its inverter grid-connected mode. Thus, its SSO problem may be limited to MSC control. By the assumptions of:

$$\begin{cases} \overline{\omega}_{tur} = \overline{\omega}_{gen} = \omega \\ \overline{T}_{tur} = J_{tur}\dot{\omega} + K\overline{\theta} \\ \overline{T}_{gen} = K\overline{\theta} - J_{gen}\dot{\omega} \\ \tilde{\omega}_{tur} = \omega_{tur} - \omega \\ \tilde{\omega}_{gen} = \omega_{gen} - \omega \\ \tilde{\theta} = \theta - \overline{\theta} \end{cases} \tag{6}$$

Equation (4) can be rewritten as:

$$\left(J_{tur} + J_{gen}\right)\dot{\omega} = \overline{T}_{tur} - \overline{T}_{gen} \tag{7a}$$

$$\ddot{\tilde{\theta}} + D\left(\frac{1}{J_{tur}} + \frac{1}{J_{gen}}\right)\dot{\tilde{\theta}} + K\left(\frac{1}{J_{tur}} + \frac{1}{J_{gen}}\right)\tilde{\theta} = \frac{1}{J_{tur}}\tilde{T}_{tur} + \frac{1}{J_{gen}}\tilde{T}_{gen} \tag{7b}$$

where the superscript "~" and "—" refer to small signal values and steady state values, respectively. Equation (7a) characterizes the rigid motion mode while (7b) reflects the resonance mode. From (7b), the flexible drive-train natural frequency is expressed as:

$$\omega_n = \sqrt{K\left(\frac{1}{J_{tur}} + \frac{1}{J_{gen}}\right)} \text{ and } f_n = \frac{\omega_n}{2\pi} \tag{8}$$

Under the drive-train parameters considered in this paper, the drive-train natural frequency is $\omega_n = 97.28$ rad/s ($f_n = 15.48$ Hz). Clearly, the natural frequency falls into the frequency range of the SSO (10–50 Hz). Rewrite (3) and (5) as:

$$T_{tur} = \overline{T}_{tur} + \underbrace{a\tilde{\beta} + b\tilde{\omega}_{tur} + c\tilde{v}}_{\approx\tilde{T}_{tur}} \tag{9a}$$

$$T_{gen} = \overline{T}_{gen} + \underbrace{\left.\frac{\partial T_{gen}}{\partial\omega_{gen}}\right|_{op}\tilde{\omega}_{gen}}_{\approx\tilde{T}_{gen}} \tag{9b}$$

where a, b and c are given in Appendix, and $\tilde{T}_{gen}$ is:

$$\tilde{T}_{gen} = \begin{cases} 2K_{opt}\omega\tilde{\omega}_{gen} > 0 & v < v_{rate} \\ -P_{rate}\tilde{\omega}_{gen}/\omega^2 < 0 & v \geq v_{rate} \end{cases} \tag{10}$$

Usually, the inertia moment has the ability to suppress speed or frequency mutation. Due to $J_{tur} >> J_{gen}$, $\tilde{\omega}_{tur} \ll \tilde{\omega}_{gen}$. This means that $\tilde{\omega}_{tur}$ can be ignored when analyzing the torsional vibration. If ω_{tur} is used for the pitch control, $\tilde{\beta}$ can also be neglected. Therefore, there are $\dot{\tilde{\theta}} \approx -\tilde{\omega}_{gen}$, $\tilde{T}_{tur} \approx c\tilde{v}$ and

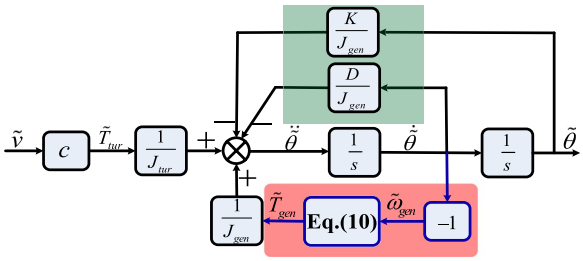

Fig. 5 Simplified small signal model

$$\ddot{\tilde{\theta}} + \frac{D}{J_{gen}}\dot{\tilde{\theta}} + \frac{K}{J_{gen}}\tilde{\theta} = \frac{1}{J_{tur}}\tilde{T}_{tur} + \frac{1}{J_{gen}}\tilde{T}_{gen} \tag{11}$$

The simplified small signal model is shown in Fig. 5. The small signal model includes the dynamics of wind turbine, drive-train, generator and its control, but does not involve the power grid and GSC control (For DFIG, it may be necessary to consider the power grid impact). In order to verify the correctness of the simplified small signal model shown in Fig. 5, a comparison between the simplified model and simulation test is conducted with the variable wind speed $v = 9 + \sin(10t)$. From the results in Fig. 6, it proves the correctness of the simplified model as the output results of the simplified model are very close to the simulation outputs in steady state.

Damping has a certain physical meaning and is expressed as the ability to block certain movements, e.g., vibration or oscillation. As Fig. 5 shows, torque control can change the system damping. If $\partial T_{gen}/\partial\omega_{gen} > 0$, the total damping can be enhanced. On the other hand, system damping is weakened if $\partial T_{gen}/\partial\omega_{gen} < 0$. From (10), the MPPT strategy with OTC can increase system damping while constant power control can weaken system damping. Therefore, SSO can occur under constant power control when the total damping is negative. Thus,

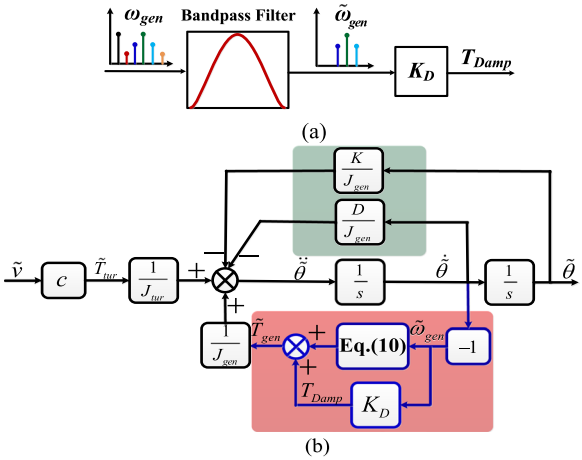

Fig. 7 Mechanism of damping control

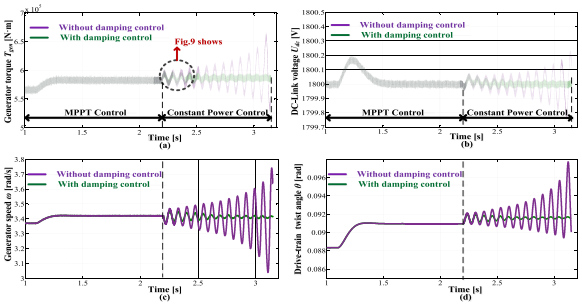

Fig. 8 System response curves. **a** Generator torque. **b** DC-Link voltage. **c** Generator speed. **d** Drive-train twist

an additional active damping control strategy must be adopted under constant power control. The mechanism of damping control method is shown in Fig. 7.

As Fig. 8 illustrates, when the system controller switched from MPPT control mode to constant power

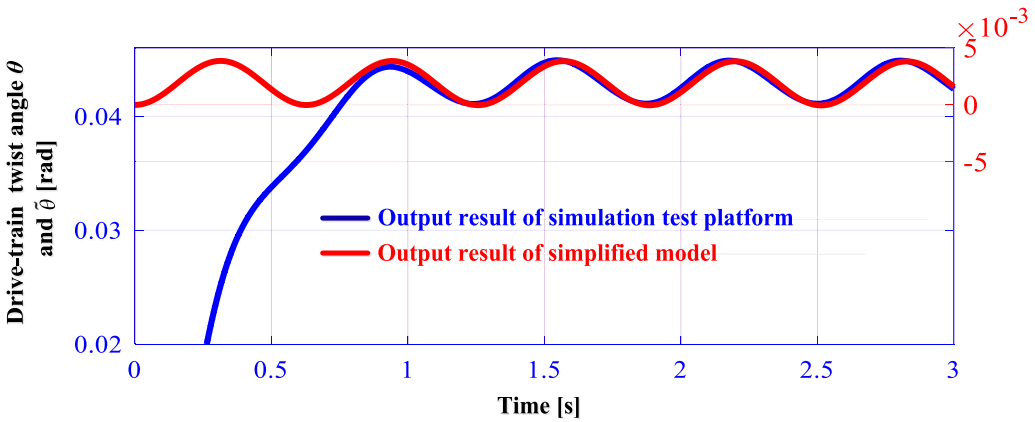

Fig. 6 Comparison between the simplified model and simulation test platform

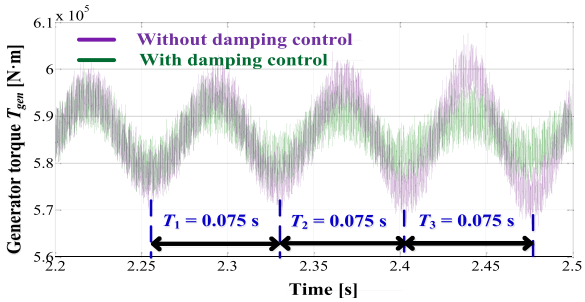

Fig. 9 Local enlarged drawing of the generator torque curve

control mode at 2.2 s, SSO occurrs without damping control and the main variables such as generator torque, DC-Link voltage, generator speed and drive-train twist angle oscillate. In contrast, after the damping control is used, SSO is completely suppressed. Figure 9 shows that the oscillation frequency (about 13.33 Hz) is close to the drive-train natural frequency.

The system power curves are shown in Fig. 10. It is evident that grid-connected power oscillation can also occur under constant power control. However, the electromagnetic power does not change much and is stable at 2 MW. The difference between the electromagnetic power and actual grid-connected power reflects the system power loss (mainly copper loss).

3.2 SSH problem analysis

From Figs. 8–10, although the system tends to be stable after adding electrical damping, the system variables have convergent oscillations in the first few cycles. This means that the under-damped system is susceptible to disturbance (e.g., wind disturbance or controller switching). Figure 11 shows the system responses to sustained excitation of periodical wind disturbance. The wind disturbance excites the oscillation of the under-damped system in the form of pulsation. This oscillation presents two frequency characteristics including under-damped oscillation (13.33 Hz) and forced oscillation caused by wind disturbance (about 3.33 Hz). By slowly increasing damping to critical damping condition, the under-damped oscillation can be completely suppressed.

From the above analyses, it can be concluded that negative damping can cause SSO and the under damping may produce SSH. In the following sections, the SSH problem will be further elaborated. It is assumed that the system is under-damped, and the disturbance produced the torsional vibration is near the drive-train natural frequency, as:

$$\tilde{\theta} = A \sin \omega_0 t \tag{12}$$

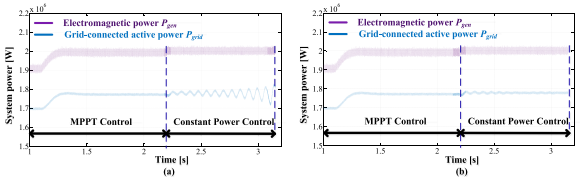

Fig. 10 Power curves. **a** Without damping control **b** With damping control

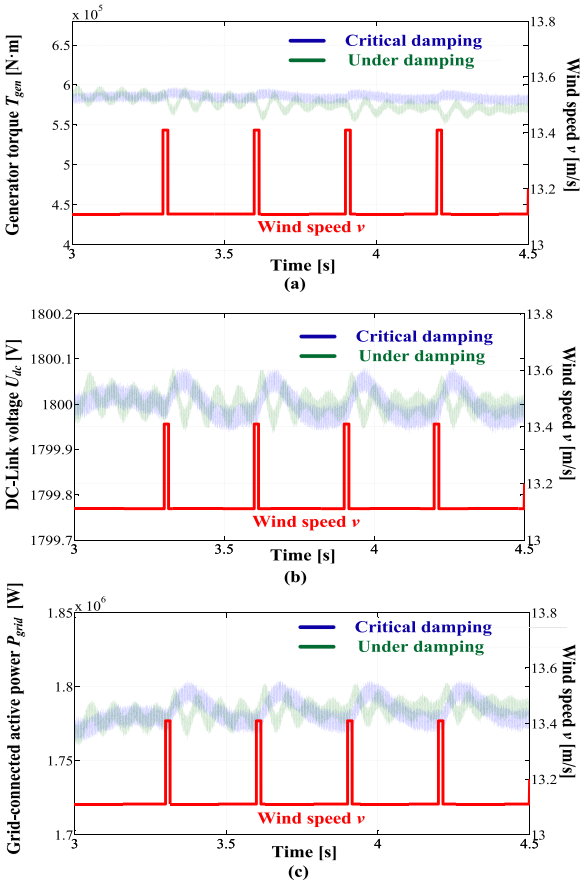

Fig. 11 System response curves. **a** Generator torque. **b** DC-Link voltage. **c** Grid-connected active power

where A is oscillation amplitude and ω_0 is oscillation frequency. In such a condition, the generator speed contains this frequency component, as:

$$\tilde{\omega}_{gen} = \tilde{\omega}_{tur} - \dot{\tilde{\theta}} \approx -\dot{\tilde{\theta}} = -A\omega_0 \cos \omega_0 t \tag{13}$$

As the electromagnetic power P_{gen} can be maintained at rated power P_{rate} (see Fig. 10), $T_{gen}=P_{gen}/\omega_{gen}=P_{rate}/\omega_{gen}$. From (10), (13), and the relationship between electromagnetic torque and q-axis stator current i_{sq}, there is:

$$\begin{aligned}\tilde{i}_{sq} &= \frac{2}{3n_p\psi}\tilde{T}_{gen} = \frac{2}{3n_p\psi}\cdot\left(-\frac{P_{rate}}{\omega^2}\tilde{\omega}_{gen}\right)\\ &= \frac{2P_{rate}A\omega_0}{3n_p\psi\omega^2}\cos\omega_0 t\end{aligned} \tag{14}$$

where n_p is a generator pole logarithm and ψ is the permanent magnet flux magnitude. From the power flow in Fig. 2, there is:

$$\begin{cases} P_{In} = P_{dc} + P_{Out} = u_{sd}i_{sd} + u_{sq}i_{sq} = u_{sq}i_{sq} \\ P_{Out} = u_{gd}i_{gd} + u_{gq}i_{gq} \\ P_{grid} = V_{gd}i_{gd} \end{cases} \tag{15}$$

where V_{gd} is the voltage at the grid-connected point. In general, the system loss mainly refers to generator copper loss, because the resistance of the coupling reactor on the grid-side is very small (assumed to be zero in this paper). Thus, the grid connection loss can be neglected and P_{Out}=P_{grid}. As Fig. 4(a) shows, if the q-axis stator current i_{sq} is fully tracking its reference i_{sq_ref}, the q-axis stator voltage u_{sq} will not contain this frequency component. Thus, there is:

$$\tilde{P}_{In} \approx \overline{u}_{sq}\tilde{i}_{sq} + \tilde{u}_{sq}\overline{i}_{sq} \approx \overline{u}_{sq}\tilde{i}_{sq} \tag{16}$$

Three scenarios in grid-side control are considered as follows:

The control function for the DC-Link voltage is very strong, and the DC-Link voltage does not fluctuate. From Fig. 4(b), when there is no fluctuation in the DC-Link voltage, $\tilde{i}_{gd} = 0$ and there is:

$$\begin{cases} \tilde{P}_{dc} = 0 \\ \tilde{P}_{grid} = \tilde{V}_{gd}\overline{i}_{gd} = \tilde{P}_{Out} = \tilde{P}_{In} = \dfrac{2P_{rate}A\omega_0\overline{u}_{sq}}{3n_p\psi\omega^2}\cos\omega_0 t \end{cases} \tag{17}$$

From (17), there is:

$$\tilde{V}_{gd} = \frac{2P_{rate}A\omega_0\overline{u}_{sq}}{3n_p\psi\omega^2\overline{i}_{gd}}\cos\omega_0 t \tag{18}$$

Equation (18) means that the voltages at the grid-connected point contain the same sub-synchronous component as the torsional vibration frequency.

The capacitor completely filters out the active power fluctuation caused by the torsional vibration., i.e.:

$$\begin{cases} \tilde{P}_{Out} = 0 \\ \tilde{P}_{dc} \approx \overline{U}_{dc}\tilde{i}_{dc} + \tilde{U}_{dc}\overline{i}_{dc} \approx C\overline{U}_{dc}\dot{\tilde{U}}_{dc} = \tilde{P}_{In} = \dfrac{2P_{rate}A\omega_0\overline{u}_{sq}}{3n_p\psi\omega^2}\cos\omega_0 t \end{cases} \tag{19}$$

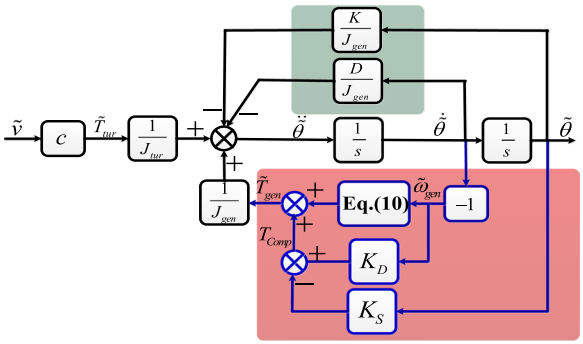

Fig. 12 Mechanism of stiffness compensation control

Thus

$$\tilde{U}_{dc} = \frac{2P_{rate}A\overline{u}_{sq}}{3n_p\psi\omega^2 C\overline{U}_{dc}}\sin\omega_0 t \tag{20}$$

From Fig. 4(b), if the lag phase of the inner-current loop is neglected, the following expression can be obtained:

$$\begin{aligned}\tilde{i}_{gd} &= \left(K_P + \frac{K_I}{s}\right)\tilde{U}_{dc} = \frac{2P_{rate}A\overline{u}_{sq}}{3n_p\psi\omega^2 C\overline{U}_{dc}}\\ &\left(K_P\sin\omega_0 t - \frac{K_I}{\omega_0}\cos\omega_0 t\right)\end{aligned} \tag{21}$$

Equation (21) indicates that the grid currents contain the same sub-synchronous component as the torsional vibration frequency.

The final case is between case 1) and case 2), i.e., both DC-Link voltage and grid-connected power fluctuate. The actual system conforms to the third situation (see Figs. 8–11), and both grid voltage and current contain SSH of this frequency.

3.3 Forced torsional vibration reduction

The study has found that increasing damping can suppress SSO and SSH, but has limited effect on suppressing the forced torsional vibration. Therefore, this paper proposes a new method by adding appropriate stiffness to reduce the forced torsional vibration. The method consists of superimposing the stiffness compensation control based on the original damping control shown in Fig. 12.

From Fig. 12, the closed-loop transfer functions can be derived as:

$$G_v(s) = \frac{\tilde{\theta}(s)}{\tilde{v}(s)} = \frac{c}{J_{tur}}G_\theta(s) \tag{22a}$$

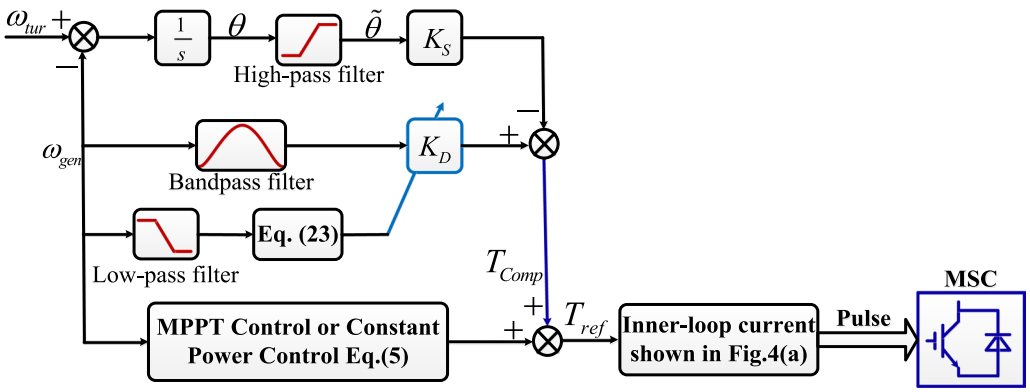

Fig. 13 Proposed control schematic to suppress forced torsional vibration

$$G_\theta(s) = \frac{1}{s^2 + \frac{1}{J_{gen}}\left(K_D + D + \frac{\partial T_{gen}}{\partial \omega_{gen}}\Big|_{op}\right)s + \frac{K+K_s}{J_{gen}}} \tag{22b}$$

Equation (22b) indicates that K_s can reduce the static gain and increase the system resonance frequency. By reducing the static gain, the forced torsional vibration caused by wind disturbance can be reduced. However, the system critical damping condition will also change:

$$K_D = 2\sqrt{J_{gen}(K+K_S)} - D - \frac{\partial T_{gen}}{\partial \omega_{gen}}\Big|_{op}, \text{ with } K_D \geq 0 \tag{23}$$

The proposed control schematic to suppress forced torsional vibration is shown in Fig. 13. Because the system needs different injection damping at different working points, the damping gain K_D should be adjusted by (23).

4 Simulation results

In order to verify the effectiveness of the proposed algorithm in this paper, a detailed simulation test platform is developed in MATLAB/SIMULINK SimPowerSysterms environment shown in Fig. 14. The transient response of PMSG-based WECS can be obtained with this simulation test platform. In this section, the focus is on the results obtained from the case study of a 2 MW PMSG-based WECS and the injected stiffness coefficient meeting $K_s = 4\,K$.

The simulation of this section consists of two tests. The first test is carried out below the rated wind speed and the wind speed curve is shown in Fig. 15(a). Thus it aims to test torsional vibration suppression under MPPT control. The system responses in these conditions are illustrated in Fig. 15. It is evident that both the conventional damping control and proposed control can effectively suppress SSH. However, compared with the conventional damping control, the proposed control method can further reduce the forced torsional vibration caused by wind disturbance, as described below.

1) Figures 15(b–d) present the curves of generator torque, DC-Link voltage and drive-train twist angle. Their fluctuations under the presented control strategy have clearly been further reduced. As is well known, drive-train twist angle fluctuation can severely damage the drive-train, and its multiplication with the stiffness coefficient has been used in many studies to characterize the shaft resonant loading. Thus, the reduction of twist angle fluctuation can help to reduce the fatigue of the drive-train.
2) Figure 15(e) shows the system power curve. As seen, the proposed control method also has the ability to reduce the fluctuations of electromagnetic power and grid connected power.
3) Although the proposed control increases speed fluctuation, the generator speed becomes closer to the rotor speed as shown in Fig. 15(f). In addition, the MPPT controller can provide positive damping to the torsional vibration. From (23), when the generator is above 1.37 rad/s, the damping gain K_D will be zero. In fact, the system only performs stiffness compensation under MPPT control and the compensation torque is shown in Fig. 15(g).

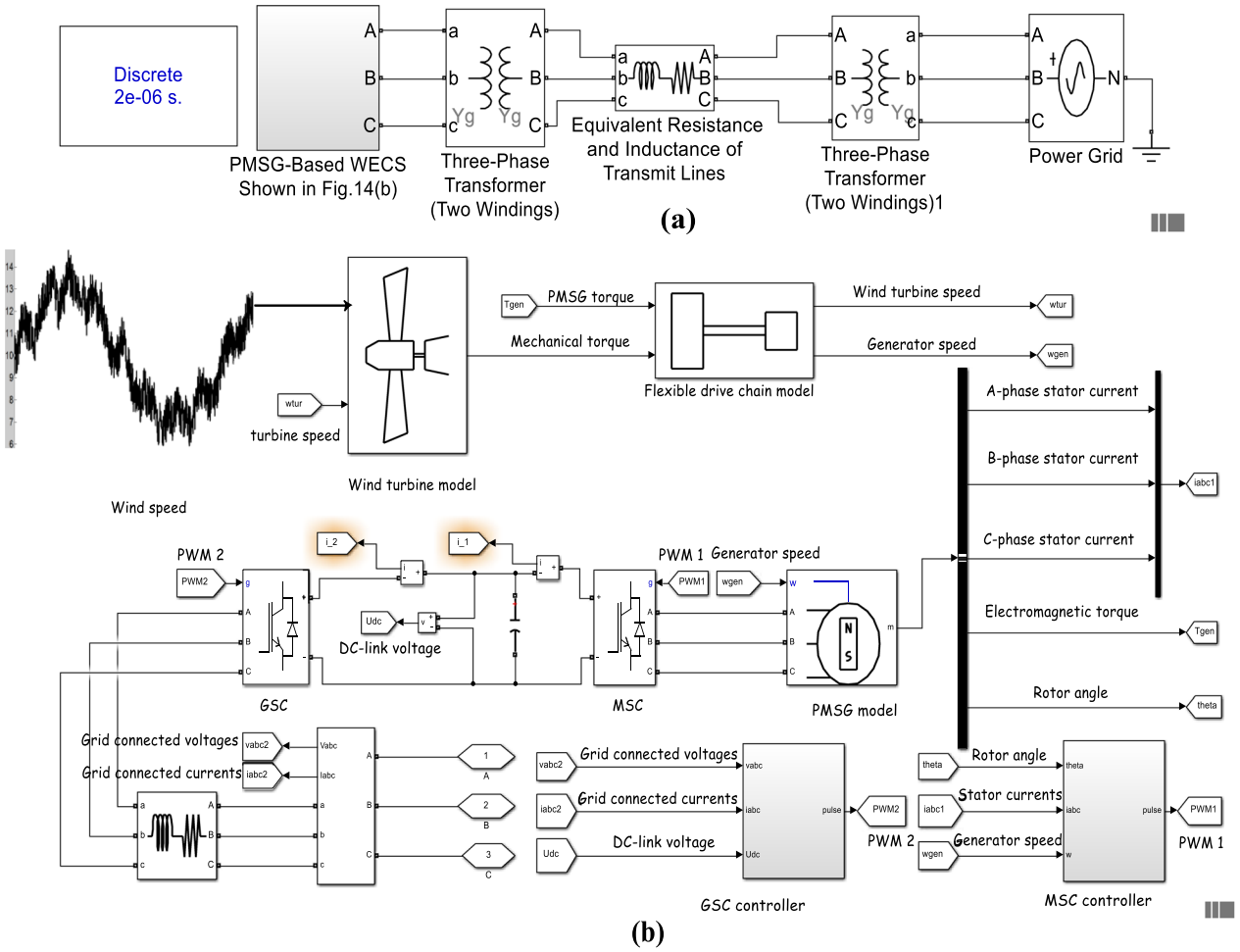

Fig. 14 Simulation test platform

The second test is implemented above the rated wind speed and the wind speed curve is shown in Fig. 16(a), while the system responses are presented in Figs. 16(b)-(g). From Figs. 16(b)-(g), the proposed control strategy is also able to reduce the forced torsional vibration under constant power control and has low fluctuations of generator torque, DC-Link voltage, drive-train twist angle and system power.

5 Conclusions

In this paper, the torsional vibration problem using MPPT control and constant power control has been studied. The hazards, causes, characteristics, conventional damping control methods and existing problems of torsional vibration are discussed. The model of the whole system and basic control of a wind turbine is presented, while the mechanisms of SSO, SSH and forced torsional vibration by wind disturbance are analyzed. A stiffness compensation control method based on adaptive damping is presented to further mitigate the forced torsional vibration. The conclusions are as follows:

1) An MPPT controller can increase system damping. However, the power controller can weaken system damping and if the total damping becomes negative, SSO will occur.

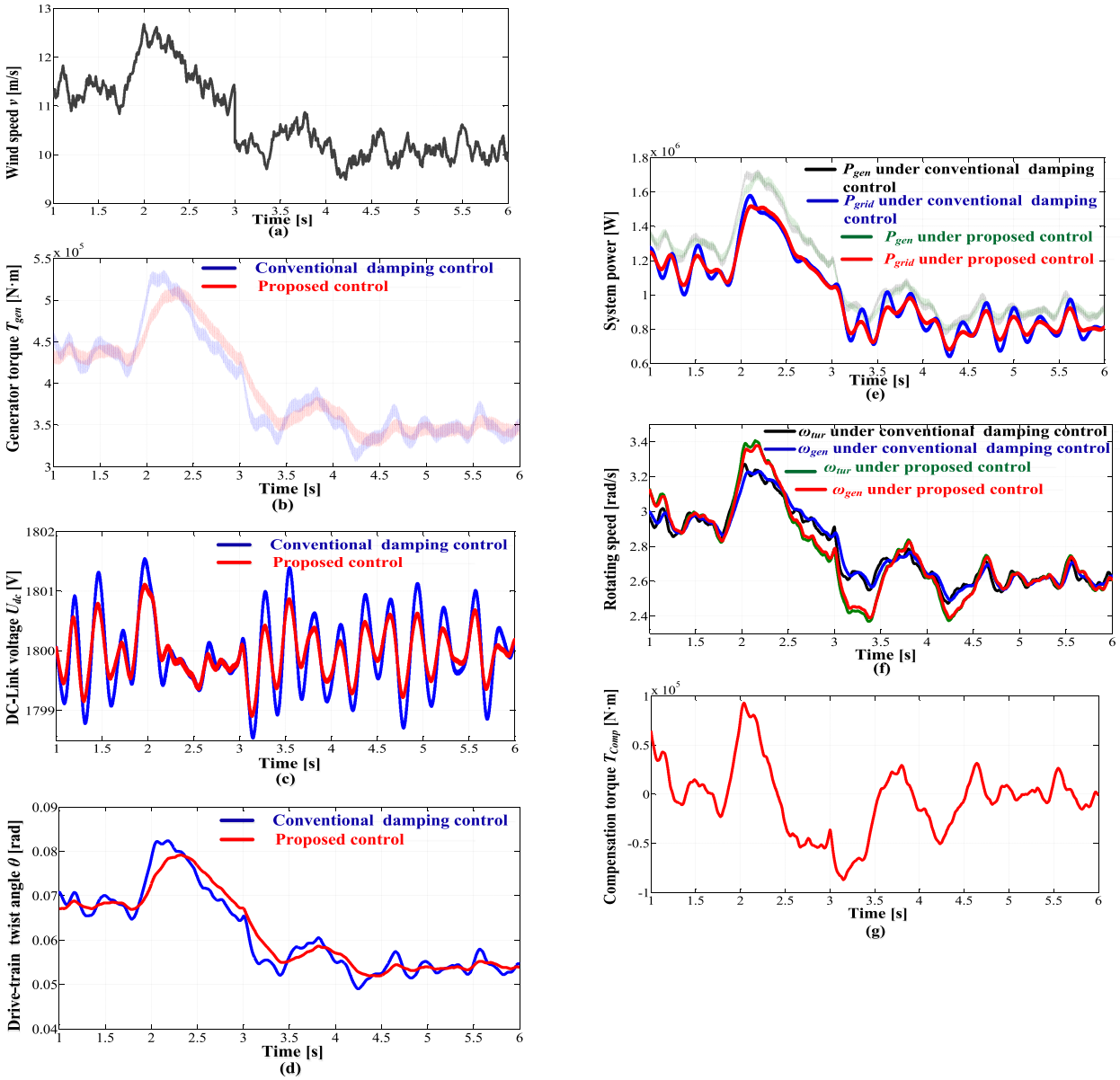

Fig. 15 Wind speed curve and system response curves below rated wind speed

2) Both MPPT control at low rotor speed (or low wind speed) and power control with insufficient damping can put the system into an under-damped state, while an under-damped system is susceptible to external disturbances to produce SSH.

3) It is found that the conventional damping control has little effect on the forced torsional vibration, but appropriate addition of stiffness can mitigate the forced torsional vibration. Therefore, the proposed new stiffness compensation control strategy based on adaptive damping can suppress forced torsional vibration.

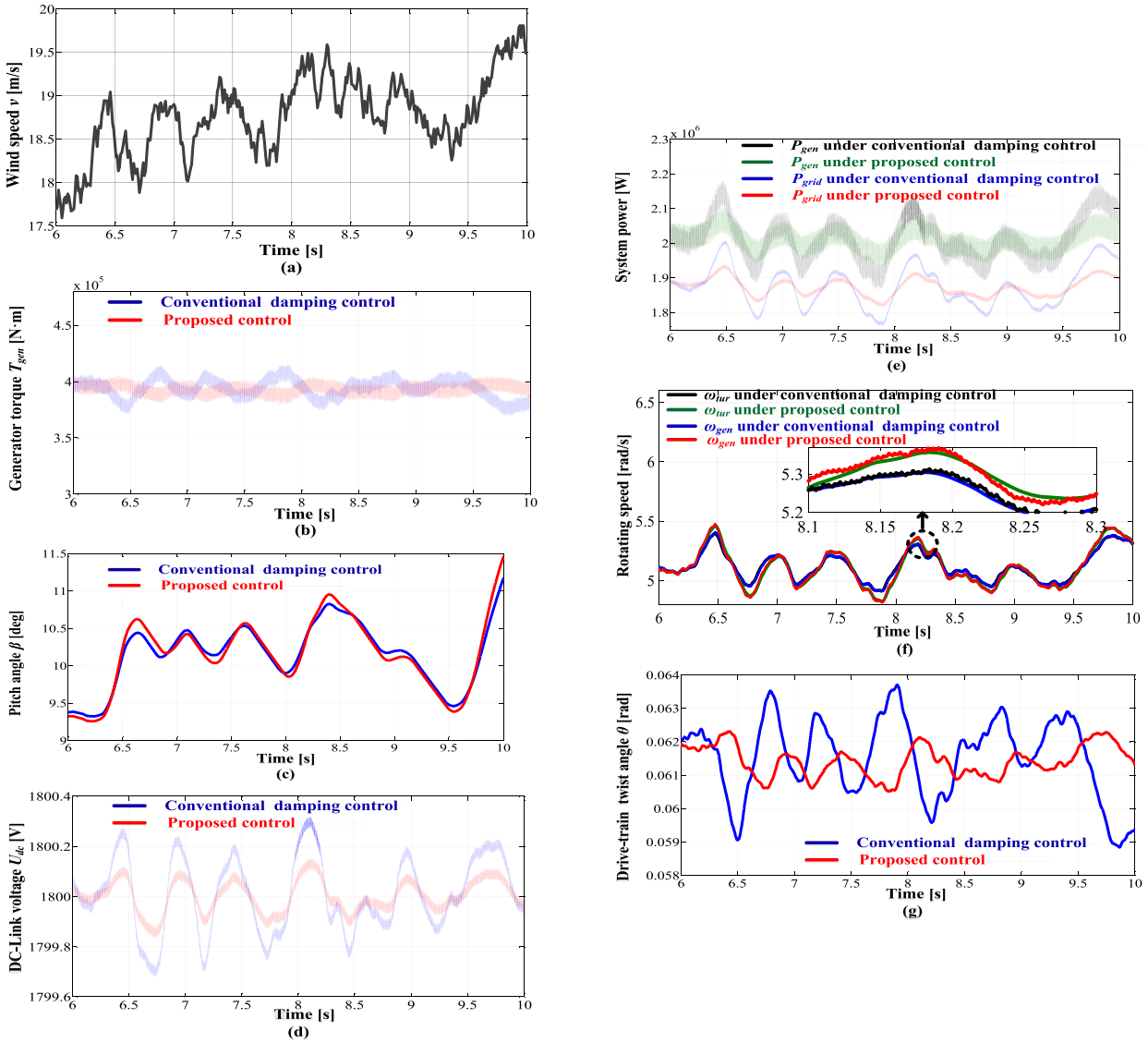

Fig. 16 Wind speed curve and system response curves above rated wind speed

Appendix

PMSG-based WECS parameters: Wind turbine inertia moment J_{tur} is 2×10^4 kg·m^2; Air density ρ is 1.225 kg/m^3; Blade length R is 31 m; Rated wind speed v_{rate} is 13.1; Generator inertia moment J_{gen} is 700 kg·m^2; Rated power P_{rate} is 2 MW; Rated torque T_{rate} is 4×10^2 kN·m; Rate rotor speed ω_{rate} is 5 rad/s; Generator pole logarithm n_p is 102; Permanent flux ϕ is 1.25 Wb; Stator-resistance is 0.11 Ω; Stator-reluctance L is 8.35 mH; DC-Link voltage U_{dc} 1800 V; Grid-side filter inductor L_c is 6 mH; Drive-train stiffness K is 6.4×10^6 N·m·s/rad; Drive-train damping D is 1.58×10^5.

Aerodynamic factors a, b, c are as follows:

$$a=\left.\frac{\partial T_{tur}}{\partial\beta}\right|_{op}=\frac{\rho\pi R^2\overline{v}^3}{2\overline{\omega}_{tur}}\cdot\frac{\partial C_P}{\partial\beta}\quad b=\left.\frac{\partial T_{tur}}{\partial\omega_{tur}}\right|_{op}=\frac{\rho\pi R^3\overline{v}^2}{2\overline{\omega}_{tur}}\left(\frac{\partial C_P}{\partial\lambda}-\frac{\overline{C}_P}{\overline{\lambda}}\right)\quad c=\left.\frac{\partial T_{tur}}{\partial v}\right|_{op}=\frac{\rho\pi R^3\overline{v}}{2}\left(\frac{3\overline{C}_P}{\overline{\lambda}}-\frac{\partial C_P}{\partial\lambda}\right)$$

Acknowledgements
Thanks to the editorial department for timely feedback, the senior duty editor and the assistant editor for handling the paper and the reviewers for the valuable comments.

Author contributions
The author systematically studied and analyzed the torsional vibration problem of PMSG-based WECS and proposed a new way to suppress the torsional vibration. The author read and approved by the final manuscript.

Authors' information
Feihang Zhou(1989-10), male, PHD. He graduated from Xi'an University of Technology in China and received the PHD degree. He is a lecturer of Xi`an University of Posts & Telecommunications now. His research focuses on the suppression of wind turbine vibration.

Funding
This work has been partially supported by Shaanxi Provincial Department of Education Project (17JK0691).

Availability of data and materials
The data used to support the findings of this study are available from the corresponding author upon request.

Declarations

Competing interests
The author declars that there are no conflicts of interest regarding the publication of this paper.

Received: 26 April 2022 Accepted: 11 August 2022
Published online: 27 September 2022

References

1. Walker, D. N., Bowler, C. E. J., Jackson, R. L., et al. (1975). Results of subsynchronous resonance test at Mohave. *IEEE Transactions on Power Apparatus and Systems, 94*(5), 1878–1889.
2. Mortensen, K., & Larsen, E. V. (1981). Field tests and analysis of torsional interaction between the coal creek turbine-generators and the CU HVDC system. *IEEE Transactions on Power Apparatus and Systems, 100*(1), 336–344.
3. Yacamimi, R. (1995). How HVDC shemes can exit torsional oscillation in turbo-alternator shafts. *Proceedings of IET Generation, Transmission and Distribution, 142*(6), 613–617.
4. Song, D., Li, Z., Wang, L., & Fangjun jin, Chaoneng Huang, E Xia, Rizk M. Rizk-Allah, Jian Yang, Mei Su, and Young Hoon Joo,. (2022). Energy capture efficiency enhancement of wind turbines via stochastic model predictive yaw control based on intelligent scenarios generation. *Applied Energy, 312*, 118773.
5. Song, D., Yanping, Tu., Wang, L., & Fangjun jin, Chaoneng Huang, Ziqun Li, E Xia, Rizk M. Rizk-Allah, Jian Yang, Mei Su, and Young Hoon Joo,. (2022). Coordinated optimization on energy capture and torque fluctuation of wind turbines via variable weight NMPC with fuzzy regulator. *Applied Energy, 312*, 118821.
6. Faried, S. O., et al. (2013). Utilizing DFIG-based wind farms for damping subsynchronous resonance in nearby turbine-generators. *IEEE Transactions on Power Systems, 28*(1), 452–459.
7. Leon, A. E., & Solsona, J. A. (2015). Sub-synchronous interaction damping control for DFIG wind turbines. *IEEE Transactions on Power Systems, 30*(1), 419–428.
8. Leon, A. E. (2017). Integration of DFIG-based wind farms into series-compensated transmission systems. *IEEE Transactions on Sustainable Energy, 7*(2), 451–460.
9. Sun, K., Yao, W., et al. (2019). Impedance modeling and stability analysis of grid-connected DFIG-based wind farm with a VSC-HVDC. *IEEE Journal of Emerging & Selected Topics in Power Electronics, 8*(2), 1375.
10. Bossanyi, E. A. (2000). The design of closed loop controllers for wind turbines. *Wind Energy, 3*(3), 149–163.
11. Bossanyi, E. A. (2003). Wind turbine control for load reduction. *Wind Energy, 6*(3), 229–244.
12. Zhang, F., Leithead, W. E. & Anaya-Lara, O. (2012). A combined controller design of power system stabilizer and wind turbine drive-train damping filter," *International Conference on Sustainable Power Generation and Supply (SUPERGEN 2012)*, pp. 1-6. https://doi.org/10.1049/cp.2012.1767.
13. Licari, J., Ugalde-Loo, C. E., Ekanayake, J. B., & Jenkins, N. (2013). Damping of torsional vibrations in a variable-speed wind turbine. *IEEE Transactions on Energy Conversion, 28*(1), 172–180.
14. Hansen, A. D., & Michalke, G. (2008). Modelling and control of variable-speed multi-pole permanent magnet synchronous generator wind turbine. *Wind Energy, 11*(5), 537–554.
15. Muszynski, R., & Deskur, J. (2010). Damping of torsional vibrations in high-dynamic industrial drives. *IEEE Transactions on Industrial Electronics, 57*(2), 544–552.
16. Mandic, G., et al. (2012). Active torque control for gearbox load reduction in a variable-speed wind turbine. *IEEE Transactions on Industry Applications, 48*(6), 2424–2432.
17. Lorenzo-Bonache, A., Honrubia-Escribano, A., Jiménez-Buendía, F., et al. (2017). Generic type 3 wind turbine model based on IEC61400-27-1: parameter analysis and transient response under voltage dips. *Energies, 10*, 1441.
18. John, L., et al. (2013). Damping of torsional vibrations in a variable-speed wind turbine. *IEEE Transactions on Energy Conversion, 28*(1), 172–180.
19. Geng, H., & Xu, D. (2011). Stability analysis and improvements for variable-speed multipole permanent magnet synchronous generator-based wind energy conversion system. *IEEE Transactions on Sustainable Energy, 2*(4), 459–467.
20. Geng, H., Xu, D., Wu, B., et al. (2011). Active damping for PMSG-based WECS with DC-link current estimation. *IEEE Transactions on Industrial Electronics, 58*(4), 1110–1119.
21. Geng, H., Yang, G., Xu, D., et al. (2011). Unified power control for PMSG-based WECS operating under different grid conditions. *IEEE Transactions on Energy Conversion, 26*(3), 822–830.
22. Chen, J., Chen, J., & Gong, C. (2014). On optimizing the aerodynamic load acting on the turbine shaft of PMSG-based direct-drive wind energy conversion system. *IEEE Transactions on Industrial Electronics, 61*(8), 4022–4031.
23. Chen, J., & Song, Y. (2015). Dynamic loads of variable-speed wind energy conversion system. *IEEE Transactions on Industrial Electronics, 63*(1), 178–188.
24. Fateh, F., White, W. N., & Gruenbacher, D. (2017). Torsional vibrations mitigation in the drivetrain of DFIG-based grid-connected wind turbine. *IEEE Transactions on Industrial Applications, 53*(6), 5760–5767.
25. Girsang, I. P., Dhupia, J. S., Muljadi, E., Singh, M., & Jonkman, J. (2013). Modeling and control to mitigate resonant load in variable-speed wind turbine drive train. *IEEE Journal of Emerging & Selected Topics in Power Electronics, 1*(4), 277–286.
26. Kambrath, J. K., Khan, M. S. U., Wang, Y., Singh, et al. (2019). A novel control technique to reduce the effects of torsional interaction in wind turbine system. *IEEE Journal of Emerging & Selected Topics in Power Electronics, 7*(3), 2009.
27. Li, Shuhui , et al. "Optimal and direct-current vector control of direct-driven PMSG wind turbines." IEEE Transactions on Power Electronics 27(5) (2012):2325–2337.
28. Mozayan, Seyed Mehdi , et al. "Sliding mode control of PMSG wind turbine based on enhanced exponential reaching law." IEEE Transactions on Industrial Electronics 63(10) (2016):6148–6159.
29. Namazi, Mohammad Masoud , et al. "Passivity-based control of switched reluctance-based wind system supplying constant power load." IEEE Transactions on Industrial Electronics (2018):1–1.
30. Morinaga, S , and T. Funabashi. Torsional vibration suppression of the PMSG-based wind turbine generator using H∞ observer. 1st International Future Energy Electronics Conference (IFEEC) (2013): 880–884.
31. Zhang, Xiaojie , W. He , and J. Hu . "Impact of Inertia control of DFIG-based WT on torsional vibration in drivetrain." IEEE Transactions on Sustainable Energy PP.99(2020):1–1.
32. F. Zhou and Jun Liu, "Pitch controller design of wind turbine based on nonlinear PI/PD control," Shock and Vibration, 2018(7859510): 14, 2018.